Synthesis mechanism of nanoporous Sn_3O_4 nanosheets by hydrothermal process without any additives*

Zhao Jun-Hua(赵俊华)[a)†], Tan Rui-Qin(谭瑞琴)[b)], Yang Ye(杨 晔)[c)], Xu Wei(许 炜)[c)], Li Jia(李 佳)[c)], Shen Wen-Feng(沈文峰)[c)], Wu Guo-Qiang(吾国强)[a)], Zhu You-Liang(朱友良)[a)], Yang Xu-Feng(杨旭峰)[a)], and Song Wei-Jie(宋伟杰)[c)]

[a)] *College of Chemical and Material Engineering, Quzhou University, Quzhou* 324000, *China*
[b)] *Faculty of Information Science and Engineering, Ningbo University, Ningbo* 315211, *China*
[c)] *Ningbo Institute of Material Technology and Engineering, Chinese Academy of Sciences, Ningbo* 315201, *China*

(Received 24 November 2014; revised manuscript received 8 January 2015; published online 10 April 2015)

Nanoporous anorthic-phase Sn_3O_4 nanosheets are successfully fabricated via a hydrothermal process without any additives. With the pH value of the precursor increasing from 2.0 to 11.8, the valence of the precursor changes from mixed valence (the ratio of Sn^{2+} to Sn^{4+} is 2.7:1) to pure bivalent, and the product transformed from Sn_3O_4 to SnO mesocrystals. When doping $SbCl_3$ to the alkaline precursor, the valence of the precursor shows mixed valence with the ratio of Sn^{2+} to Sn^{4+} being 2.6:1 and Sn_3O_4 is synthesized after the hydrothermal process. The valence state of Sn species in the precursor is the key factor of the formation of Sn_3O_4. The synthesis mechanism is discussed and proposed. These experimental results expand the knowledge base that can be used to guide technological applications of intermediate tin oxide materials.

Keywords: Sn_3O_4 nanosheets, hydrothermal synthesis, valence control, precursor

PACS: 62.23.Kn, 61.46.Hk, 61.82.Rx **DOI:** 10.1088/1674-1056/24/6/066202

1. Introduction

Mixed-valence oxide materials show unique properties and broad application prospects, such as catalysis,[1–3] sensors,[4,5] electronics industry,[6,7] magnetic shielding materials,[8–10] and so on. Intermediate tin oxides SnO_{2-x} ($0 < x < 1$), such as Sn_5O_6, Sn_3O_4, and Sn_2O_3, enrich the material performances and application fields of advanced functional tin oxide materials, receiving increasing attention.[11,12] Sn_3O_4 is one of the important heterovalent tin oxides and generally remains in theoretical calculations.[13,14] Sn_3O_4 nanoparticles prepared by decomposition of SnO or carbothermal reduction of SnO_2 are accompanied by stoichiometric tin oxides or metallic tin.[13,15,16] We have reported the pure phase of Sn_3O_4 nanosheets synthesized by the hydrothermal method.[11,17] To the best of our knowledge, there are very few reports about the synthesis mechanism of pure mixed-valence crystalline phase of Sn_3O_4.

In this paper, nanoporous Sn_3O_4 nanosheets are prepared by the hydrothermal process without any additives. Through the experimental study and the theoretical analysis, the synthesis mechanism of Sn_3O_4 nanosheets is proposed and analyzed.

2. Experiment

All reagents were analytically pure, purchased from Sinopharm Chemical Reagent Co. Ltd, and directly used without further purification. In a typical procedure, the Sn^{2+} precursor ($SnCl_2{\cdot}2H_2O$, 8 mmol) was dissolved in distilled water by vigorous magnetic stirring.[11] The pH of the system was adjusted with 0.5-M sodium hydroxide to acidic conditions (pH = 2.0) at room temperature (sample 1). The obtained mixture was under continuous magnetic stirring for 1 h and then transferred into a Teflon-lined stainless steel autoclave, sealed and maintained at 180 °C for 12 h. A kind of light-blue precipitate was collected, washed with distilled water and ethanol respectively until Cl^- could not be detected. The products were finally dried in air at 60 °C. Sample 2 was synthesized in alkali medium (pH = 11.8) and adjusted with 0.5-M sodium hydroxide. Sample 3 was synthesized by adding 0.48-mmol antimony in the precursor of sample 2.

The phase identification was performed by x-ray diffraction (XRD) using a Bruker AXS D8 advance diffractometer with Cu $K\alpha$ radiation at a power of 1.6 kW. High-resolution transmission electron microscopy (HRTEM) studies were carried out with an FEI Tecnai F20 field emission electron microscope. The x-ray photoelectron spectroscopy (XPS) spectra were obtained by the Kratos Axis Ultra DLD XPS system. The optical transmission spectra were recorded with an ultraviolet-visible-near-infrared (UV-visible-NIR) spectrometer (Perkin Elmer Lambda 950, Shelton, USA) in a wavelength range of 220 nm–240 nm.

*Project supported by the National Natural Science Foundation of China (Grant Nos. 21377063, 51102250, 21203226, and 21205127) and the Personnel Training Foundation of Quzhou University (Grant No. BSYJ201412).

†Corresponding author. E-mail: Zhaojh1018@163.com

© 2015 Chinese Physical Society and IOP Publishing Ltd

3. Results and discussion

3.1. Structural and morphology analysis

Figure 1(a) shows the typical XRD pattern of the as-synthesized nanocrystals (sample 1). It could be observed that all diffraction peaks can be indexed to the anorthic-phase Sn_3O_4 (JCPDS No. 16-0737). No additional impurity diffraction peaks are observed, which indicates that the single-phase Sn_3O_4 is obtained in the present work. As shown in the higher-magnification SEM and TEM images in Fig. 1(b), the Sn_3O_4 shows a sheet-like shape with a thickness of about 10 nm∼20 nm. The selected-area electron diffraction (SAED) pattern shows a single-crystal-like diffraction corresponding to the [010] zone axis. It is shown in Fig. 1(c) that the plate has a (101) interplanar distance of 0.372 nm and a (002) interplanar distance of 0.242 nm. The XPS measurements demonstrate that the area ratio of $S(Sn^{2+})/[S(Sn^{4+})+S(Sn^{2+})]$ is 0.66 deduced from the Sn 3d spectra (Fig. 1(d)). This is in good agreement with the theoretical value of 0.67 in Sn_3O_4. The Brunauer–Emmett–Teller (BET) surface area of the single-crystal-like nanosheet is further investigated by N_2 adsorption–desorption measurements in Fig. 2. The representative nitrogen isotherm shows a uniform pore size distribution with an average pore diameter of 2.3 nm and a high surface area of 67 m^2/g. The regions of low contrast between individual crystallites (Fig. 1(c)) indicate mesopores with diameters of about 1.2 nm∼2.7 nm,[18,19] which is in good agreement with the pore size distribution results. Considering all the above results, it can be concluded that nanoporous anorthic-phase Sn_3O_4 nanosheets have been successfully fabricated by the hydrothermal process without any additives.

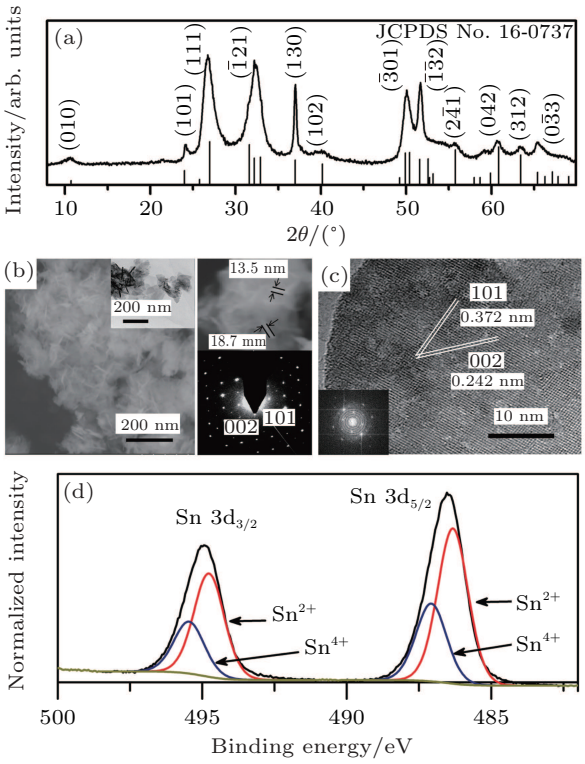


Fig. 1. (color online) XRD pattern (a), SEM (b), HRTEM image (c), and XPS (d) of nanoporous Sn_3O_4 nanosheets. The upper left inset in panel (b) shows the TEM image, the upper right inset is the SEM image, and the lower right inset is the SAED pattern.

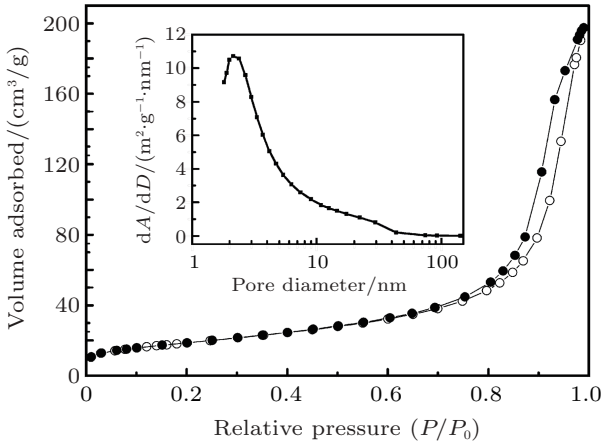


Fig. 2. N_2 adsorption–desorption isotherms of nanoporous anorthic Sn_3O_4 mesocrystals. The solid and empty symbols represent adsorption and desorption data, respectively. The inset shows the pore size distribution obtained from the adsorption branch.

3.2. Synthesize mechanism of Sn_3O_4 nanosheets

It should be noted that SnO mesocrystals are synthesized in the same fabrication progress when the pH is adjusted to 11.8 by sodium hydroxide (sample 2).[20] For investigating the formation mechanism of the Sn_3O_4, the precursors of different pH values during the reaction are monitored. Powder XRD patterns in Fig. 3 indicate that the precursor prepared with a pH value of 11.8 is consistent with the standard $Sn_6O_4(OH)_4$, and the precursor prepared with a pH value of 2.0 is similar to $Sn_6O_4(OH)_4$ with peaks shifting toward higher angles. According to the XPS measurements (Fig. 4), chemical states of the tin elements of the precursor prepared in an alkaline condition (sample 2) are all bivalent while those prepared in an acidic condition (sample 1) are mixed valence with a ratio of Sn^{2+} to Sn^{4+} being 2.7:1.

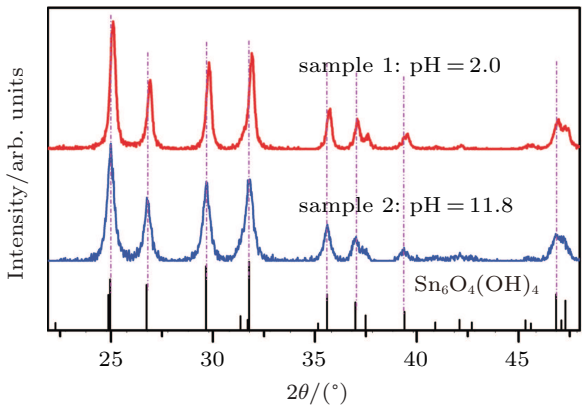


Fig. 3. (color online) Typical XRD pattern of the precursor of samples 1 and 2.

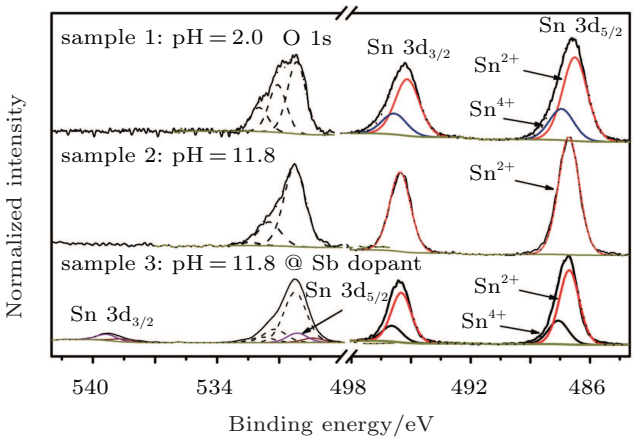


Fig. 4. (color online) The Sn 3d and Sb 3d XPS spectra of the precursors for samples 1, 2, and 3.

To clearly identify the synthesis mechanism of Sn_3O_4 nanosheets, a comparative experiment is carried out. A controlled-valence progress is introduced to regulate the valence of the precursor to synthesize Sn_3O_4 nanosheets in an alkaline condition. Verwey *et al.* have successfully changed the valence of Ti^{4+} or Mn^{4+} in $CaTiO_3$ or $CaMnO_3$ respectively by La dopant.[21] In our comparative experiment, antimony (6 at.%) is considered to be doped into the precursor and the pH value is adjusted to 11.8 by sodium hydroxide (sample 3). The chemical states of the two principal elements (Sn and Sb) in sample 3 are characterized by XPS. In the precursor of sample 3, the ratio of Sn^{2+} to Sn^{4+} is 2.6:1 and the ratio of Sb^{3+} to Sb^{5+} is 1.6:1 (Fig. 4). Figure 5 shows the XRD pattern of sample 3. As-synthesized particles exhibit a perfectly anorthic-phase Sn_3O_4 structure (JCPDS No. 16-0737). According to the data mentioned above, the valence state of Sn species in the precursor might be the key factor of the formation of Sn_3O_4 nanosheets.

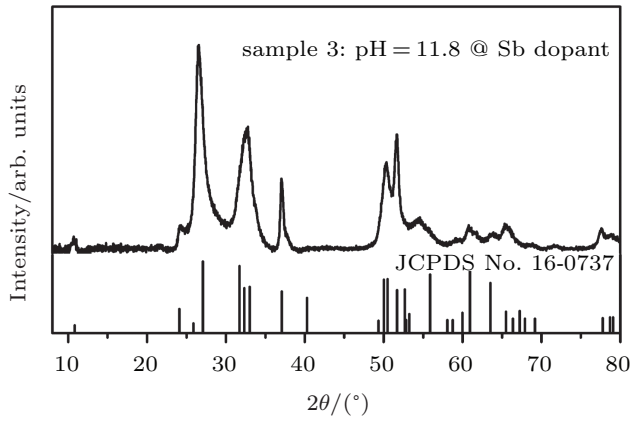


Fig. 5. Typical XRD pattern of sample 3 with 6 at.% Sb doping and 11.8-pH value.

The hydrolysis process of sample 3 is monitored by UV-vis. The reaction is stable for about 20 min (Fig. 6(a)) and the satellite peak below the absorption edge evolves from one to two near 225 nm and 228 nm, which correspond to the formation of Sn^{4+} species.[22] However, for sample 2 (Fig. 6(b)), the hydrolysis process of $SnCl_2$ lasts for 5 min with no Sn^{4+} spices existing in the precursor. It indicates that the $SbCl_3$ not only slows the hydrolysis rate of $SnCl_2$ but also facilitates the oxidization of Sn(2). The reaction scheme of the dissolution of $SnCl_2$ in an alkaline condition is as follows:

$$6SnCl_2 + 12OH^- \rightarrow Sn_6O_4(OH)_4 + 12Cl^- + 4H_2O. \quad (1)$$

With the addition of $SbCl_3$ in sample 3, the rate of hydrolysis of $SnCl_2$ is slowed down according to the following reaction:[23,24]

$$SnCl_2 + SbCl_3 \rightarrow SbCl_2^+ + SnCl_3^-. \quad (2)$$

The system becomes unstable and the Sn(2) and Sb(3) ions are slowly oxidized to Sn(4) and Sb(5) in air under magnetic stirring. After the precursor transforms into a Teflon-lined autoclave, the Sn(2) and Sb(3) are continuously oxidized by oxygen molecules in the hydrothermal environment. The oxygen molecules come from the air (30 mL) in the Teflon container and are dissolved in the precursor solution ($[O_2] \approx 1.4$ mM).[25] However, the oxygen molecules in the system are insufficient for totally oxidizing the Sn(2) species, with an upper limit yield of 35.8 mol%. Sn_3O_4 has the most stable structure in SnO_{2-x} ($x = 0.73$–0.60) and has a formation energy of -9 meV/Sn.[14] Thus, Sn_3O_4 is formed finally in an alkaline condition.

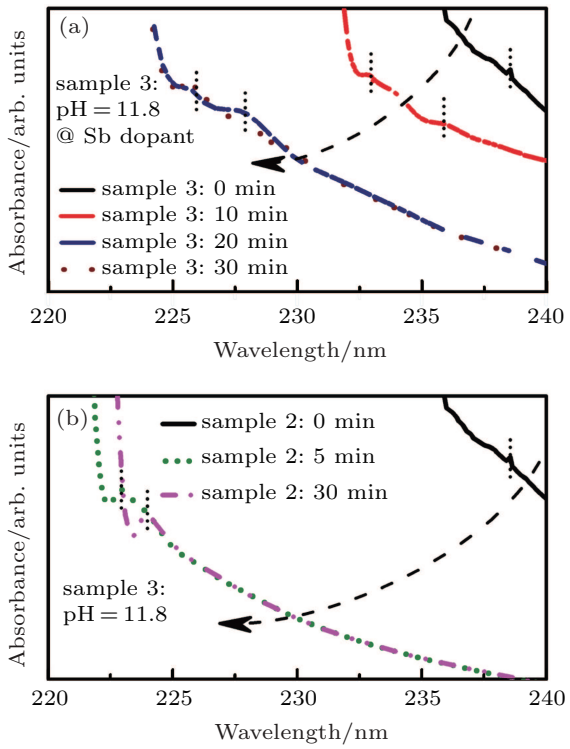


Fig. 6. (color online) UV-vis spectra of the hydrolysis process of samples 3 (a) and 2 (b) with different reaction times.

4. Conclusions

In this study, nanoporous anorthic-phase Sn_3O_4 nanosheets are successfully fabricated by a hydrothermal process without any additives. As-synthesized nanosheets exhibit a dominant exposed plane of [010], an average pore diameter of 2.3 nm, and a high surface area of 67 m^2/g. The valence of precursor changes from mixed valence with a ratio of Sn^{2+} to Sn^{4+} being 2.7:1 to pure bivalent, when the pH value of the precursor increases from 2.0 to 11.8. The precursor is pure bivalent synthesized SnO mesocrystals instead of Sn_3O_4. In this alkaline atmosphere, a controlled-valence process is introduced to regulate the valence of the precursor to mixed valence with a ratio of Sn^{2+} to Sn^{4+} being 2.6:1 by doping Sb atoms. This Sb-doped precursor is oxidized into pure Sn_3O_4 phase after the hydrothermal process. The synthesis mechanism is proposed and characterized. These fundamental researches can enrich the knowledge base and are important for the technological applications of intermediate tin oxide materials.

References

[1] Parkinson G S, Novotny Z, Argentero G, Schmid M, Pavelec J, Kosak R, Blaha P and Diebold U 2013 *Nat. Mater.* **12** 724
[2] Liu F, Zhu J H, Hou Y L and Gao S 2013 *Chin. Phys. B* **22** 107503
[3] Cai P, Chen H M and Xie J 2014 *Chin. Phys. B* **23** 117504
[4] Ahn H, Park H, Joo J C and Kim D J 2013 *ECS Solid State Lett.* **2** 11
[5] Xue D S, Zhang L Y, Gao C X, Xu X F and Gui A B 2004 *Chin. Phys. Lett.* **21** 733
[6] Bou A, Torchio Ph, Barakel D, Thierry F, Sangar A, Thoulon P Y and Ricci M 2014 *J. Appl. Phys.* **116** 023105
[7] Luo B C, Chen C L and Xie L 2011 *Acta Phys. Sin.* **60** 027306 (in Chinese)
[8] Hu Y, Li J C, Shen M W and Shi X Y 2014 *Chin. Phys. B* **23** 078704
[9] Zeng J F, Jing L H, Hou Y, Jiao M X, Qiao R R, Jia Q J, Liu C Y, Fang F, Lei H and Gao M Y 2014 *Adv. Mater.* **26** 2694
[10] Lei J M, Lv L, Liu L and Xu X L 2011 *Acta Phys. Sin.* **60** 017501 (in Chinese)
[11] Zhao J H, Tan R Q, Shen W F, Yang Y, Guo Y Q, Li J, Zhou Z, Jian J W and Song W J 2012 *Mater. Lett.* **84** 94
[12] Zhu J, Lei D N, Zhang G H, Li Q H, Lu B G and Wang T H 2013 *Nanoscale* **5** 5499
[13] Lawson F 1967 *Nature* **215** 955
[14] Seko A, Togo A, Oba F and Tanaka I 2008 *Phys. Rev. Lett.* **100** 045702
[15] White T A, Moreno M S and Midgley P A 2010 *Z. Kristallogr.* **225** 56
[16] Berengue O M, Simon R A, Chiquito A J, Dalmaschio C J, Leite E R, Uerreiro G H A and Guimaraes F E G 2010 *J. Appl. Phys.* **107** 033717
[17] Xu W, Li M, Chen X B, Zhao J H, Tan R Q, Li R, Li J and Song W J 2014 *Mater. Lett.* **120** 140
[18] Zhou L, Smyth-Boyle D and O'Brien P 2008 *J. Am. Chem. Soc.* **130** 1309
[19] Li L and Liu C Y 2010 *CrystEngComm* **12** 2073
[20] Zhao J H, Tan R Q, Guo Y Q, Lu Y H, Xu W and Song W J 2012 *CrystEngComm* **14** 4575
[21] Verwey E J W, Haaijman P W, Romeijn F C and Van Oosterhout G W 1950 *Philips Res. Rep.* **5** 173
[22] Popescu D A, Herrmann J M, Ensuque A and Verduraz F B 2001 *Phys. Chem. Chem. Phys.* **3** 2522
[23] Habboush D A and Osteryoung R A 1984 *Inorg. Chem.* **23** 1726
[24] Whitney J E and Davidson N 1949 *J. Am. Chem. Soc.* **71** 3809
[25] Uchiyama H, Ohgi H and Imai H 2006 *Cryst. Growth Des.* **6** 2186